ELSEVIER

Earth and Planetary Science Letters 198 (2002) 113–127

EPSL

www.elsevier.com/locate/epsl

Does thermal weakening explain basin inversion? Stochastic modelling of the thermal structure beneath sedimentary basins

D.L. Hansen *, S.B. Nielsen

University of Aarhus, Department of Earth Sciences, Finlandsgade 6–8, DK-8200 Aarhus N, Denmark

Received 21 June 2000; received in revised form 12 December 2001; accepted 3 January 2002

Abstract

The fact that basin inversion is possible long after the cessation of rifting indicates that at least some sedimentary basins are characterized by permanent relative weakness. This paper investigates whether the steady-state thermal structure in itself can provide the necessary pattern of rheological weakening to facilitate compressional inversion of a sedimentary basin. By Monte Carlo simulation of a two-dimensional thermal finite element model we find that, generally, the maximum Moho temperature, and therefore also the weakest upper mantle, is encountered beneath the flanks of the basin. The reason for this is heat refraction deviating away from the central parts of the sedimentary cover and into the adjacent basement highs. The weakest crust, however, is located in the center of the basin due to sediment thermal blanketing, lower confining pressure, and the presence of relatively weak sediments.

Keywords: basin inversion; thermal properties; lithosphere; rheology; Monte Carlo analysis

1. Introduction

In recent years the phenomenon of basin inversion has drawn attention to the mechanical state of sedimentary basins. The term 'inversion' refers to the reversal of vertical displacements of the subsedimentary basement of sedimentary basins and the coeval transformation of normal faults into reverse faults [1]. During the tectonic process of sedimentary basin inversion the deepest parts of basins are uplifted and sediments eroded. Inversion is accompanied by the simultaneous formation of marginal troughs on the former rift shoulders [2].

Basin inversion is a consequence of lithospheric compression and inverted basins are often found in orogenic forelands as in the case of the Alpine foreland in north-western Europe [3]. Here, in a relatively young and heterogeneous lithosphere, inversion structures are found at distances of up to 1300 km from the Alpine orogen. Some are related to Mesozoic wrench-induced sedimentary basins such as the Polish Trough, the Sole Pit Basin, Lower Saxony Basin and the Weald Basin

* Corresponding author.
E-mail addresses: david@geo.aau.dk (D.L. Hansen), sbn@geo.aau.dk (S.B. Nielsen).

0012-821X/02/$ – see front matter
PII: S0012-821X(02)00471-5

while others formed by transpressional uplift of basement blocks such as the Lusatian Block and the Bohemian Massif [4]. Most of the inverted basins in the Alpine foreland show considerable two-dimensionality being several hundreds kilometers long and only few tens of kilometers wide.

Since the lithosphere deforms where it is weakest, the phenomenon of basin inversion indicates that at least some sedimentary basins represent relatively weak parts of the continental lithosphere. The reason for this apparent weakness has been the subject of much debate [2,3,5] and is also the subject of this study.

The formation of sedimentary basins in extension or transtension results in crustal thinning which brings upper mantle material closer to the surface. This generally causes mantle temperatures to decrease and the integrated strength to increase. Even after complete thermal relaxation and sediment loading the upper mantle is still at a shallower depth than before stretching. From this observation arises the paradox of basin inversion. Why do compressional intra-plate deformations localize in sedimentary basins when theory predicts that upper mantle material beneath basin centers is relatively cold and strong in comparison with the surrounding mantle material?

The possibility of sedimentary basins being characterized by structural weakness in the form of faults and shear zones has been suggested [3]. Two-dimensional rheological finite element models including permanent structural weak zones have been used to model the formation and subsequent inversion of sedimentary basins [2]. In this latter study of Nielsen and Hansen [2] uplift of the basin center is accounted for by crustal thickening, while the marginal troughs are caused by load-induced flexure of the upper mantle. The results of this conceptually simple model in which crustal weak zones are used in basin formation and later reused in compression shows considerable agreement with observations. The model does not, however, account for the origin of the zones of structural weakness.

Recently, Sandiford [5] suggested that basin inversion can be the result of thermal weakening. His study was based on a one-dimensional consideration of the thermal state of thermally equilibrated extensional basins and led to the conclusion that thermal weakening of the upper mantle may provide a plausible physical basis for the common occurrence of inversion structures formed long after cessation of rifting. It was argued that in many cases, the steady-state temperature of the crust–mantle transition can be expected to be higher beneath the center of a thermally equilibrated extensional basin than in the unstretched lithosphere of the pre-rift situation because of the thermal blanketing effect of low conductive sediments and the burial of heat-producing upper crust. However, this finding does not agree well with detailed two- and three-dimensional thermal and thermo-mechanical studies of sedimentary basins in north-west Europe [6,7]. In these studies, lithospheric mantle beneath sedimentary basins appears to be relatively strong because it is relatively cold at equilibrium. Also, inverse thermal modeling in the Danish part of the eastern North Sea area clearly reveals a relatively cold and strong upper mantle beneath the Norwegian–Danish Basin [7].

In this study we will test the robustness of the hypothesis of thermal weakening using more realistic two-dimensional models. By the use of Monte Carlo simulation we will describe the necessary conditions for thermal weakening to occur. It will become apparent that the one-dimensional approximation is generally not well suited for the description of the thermal state of sedimentary basins, and that it will often result in misleading conclusions.

2. The thermal state of sedimentary basins

In most cases the period from rift cessation to compressional inversion of sedimentary basins in the Alpine foreland exceeds the lithospheric thermal time constant ($\simeq 60$ Ma). Furthermore, thermal blanketing by the sediments filling the rift greatly reduces the excess heat loss of the lithosphere during and after stretching. Therefore, it is reasonable to assume that basins in the Alpine foreland generally must have been close to thermal equilibrium at the time of inversion [3,5]. In

cases where the time separation between rifting and compression is less, thermal transients must be considered [8].

The continental lithosphere is often assumed to deform as a rheologically layered structure by elastic, plastic and viscous rheologies [9,10]. Elasto-plastic rheologies dominate in the upper part of the crust where yield strength is primarily dependent on confining pressure and the existence and orientation of crustal discontinuities such as faults and shear zones. Beneath the brittle–ductile transition temperature-dependent viscous creep act to relax deviatoric stresses. Often creep in the lithosphere is described by a power law, which states that creep stress (σ) depends on strain rate ($\dot{\varepsilon}$), mineralogic creep parameters (B, Q, n) and temperature (T) in the following way [10]:

$$\sigma = 2B\dot{\varepsilon}^{1/n}\exp\left(\frac{Q}{nRT}\right) \quad (1)$$

where R is the gas constant. Assuming lateral homogeneity of mineralogical creep parameters, the temperature variation at a petrological boundary like the Moho is a direct indicator of lateral strength variation in the upper mantle. Therefore, the temperatures at petrological boundaries such as the mid-crustal and the crust–mantle (Moho) transitions are very important geodynamic parameters.

As pointed out by Sandiford [5] the process of extensional basin formation produces several strength-reducing effects which counteract the strength increase associated with Moho elevation. First of all the presence of sediments (characterized by relatively low thermal conductivities) increases the near-surface geothermal gradients and thereby heat the underlying lithosphere by thermal blanketing. Secondly, the burial of heat-producing crustal material also increases the temperature of the underlying lithosphere, and is indeed a consequence of crustal thinning, if heat production is concentrated within the uppermost part of the crust. Therefore, the resulting temperature change following basin formation of the uppermost part of the mantle is a consequence of competing effects. In the following, we concentrate on temperature changes at the crust–mantle transition resulting from the basin-forming process. The resulting strength variations of crustal material are also discussed below.

3. Monte Carlo simulations

A comprehensive description of the equilibrium thermal state of sedimentary basins involves many parameters, which all to varying degrees influence the upper mantle temperature and thereby contribute to either thermal strengthening or thermal weakening. In order to unravel the effects of the different parameters we have resorted to the method of Monte Carlo simulation.

In the following an assemblage of general equations describing the configuration of a class of sedimentary basins are established. The equations are based on simple considerations and well known principles from basin analysis.

The shape of basement topography ($Z_b(x)$) of a sedimentary basin is approximated by a simple Gaussian function:

$$Z_b(x) = Z_s\exp[-(x/L_{1/2})^2] \quad (2)$$

where Z_s is the sediment thickness in the basin center, x is horizontal distance and $L_{1/2}$ is the characteristic basin half width.

Assuming Airy isostasy and uniform stretching of the entire crust, the sediment thickness in the basin center after rifting and long-term post-extensional sediment-loaded subsidence can be related to the stretching factor by:

$$Z_s \approx Z_c\left(1-\frac{1}{\beta}\right)\frac{\rho_m-\rho_c}{\rho_m-\langle\rho_s\rangle} \quad (3)$$

where Z_c is the crustal thickness before stretching, β is the stretching factor, and ρ_m and ρ_c are average densities of mantle and crustal material, respectively. $\langle\rho_s\rangle$ is the average density of sediments at the basin center obtained by:

$$\langle\rho_s\rangle = \langle\phi\rangle\rho_w + (1-\langle\phi\rangle)\rho_g \quad (4)$$

$$\langle\phi\rangle = \frac{\phi_0}{cZ_s}(1-e^{-cZ_s}) \quad (5)$$

where $\langle\phi\rangle$ is the average value of a depth-dependent porosity ($\phi(z)=\phi_0 e^{-cz}$) [11].

We assume that sedimentary parameters such as surface porosity (ϕ_0), compaction coefficient (c) and sediment grain density (ρ_g) can be expressed as linear combinations of parameters related to two end-member lithologies (sandstone and shale):

$$\rho_g = \Theta\rho_g^{\text{shale}} + (1-\Theta)\rho_g^{\text{sandstone}} \quad (6)$$

$$\phi_0 = \Theta\phi_0^{\text{shale}} + (1-\Theta)\phi_0^{\text{sandstone}} \quad (7)$$

$$c = \Theta c^{\text{shale}} + (1-\Theta)c^{\text{sandstone}} \quad (8)$$

where $\Theta\in[0,1]$ is the shale fraction.

Similarly, the average thermal conductivity of the sediment matrix (k_g) is expressed as a linear combination of the thermal conductivities of sandstone and shale matrix:

$$k_g = \Theta k_g^{\text{shale}} + (1-\Theta)k_g^{\text{sandstone}} \quad (9)$$

The average thermal conductivity of the basin fill (sediment matrix and pore fluid) $\langle k_s\rangle$ is, due to the spatially distribution of porosity, best described by the geometric mixing law:

$$\langle k_s\rangle = k_g\left(\frac{k_w}{k_g}\right)^{\langle\phi\rangle} \quad (10)$$

Table 1
Fixed parameter values

Symbol	Parameter	Value
$L_{1/2}$	Basin half width	40 km
ρ_m	Density of mantle	3200 kg/m^3
ρ_c	Average density of crust	2800 kg/m^3
ρ_g^{shale}	Grain density of shale	2750 kg/m^3
ρ_g^{sand}	Grain density of sandstone	2650 kg/m^3
ρ_w	Density of water	1000 kg/m^3
ϕ_0^{shale}	Surface porosity of shale	0.63
ϕ_0^{sand}	Surface porosity of sandstone	0.49
c^{shale}	Comp. coef. of shale	0.50 km^{-1}
c^{sand}	Comp. coef. of sandstone	0.27 km^{-1}
k_g^{shale}	Grain conductivity of shale	1.0 W/(mK)
k_g^{sand}	Grain conductivity of sandstone	4.0 W/(mK)
k_w	Conductivity of water	0.6 W/(mK)
A_s	Sedimentary heat production	1.0 μW/m^3

For explanations see Eqs. 2–12.

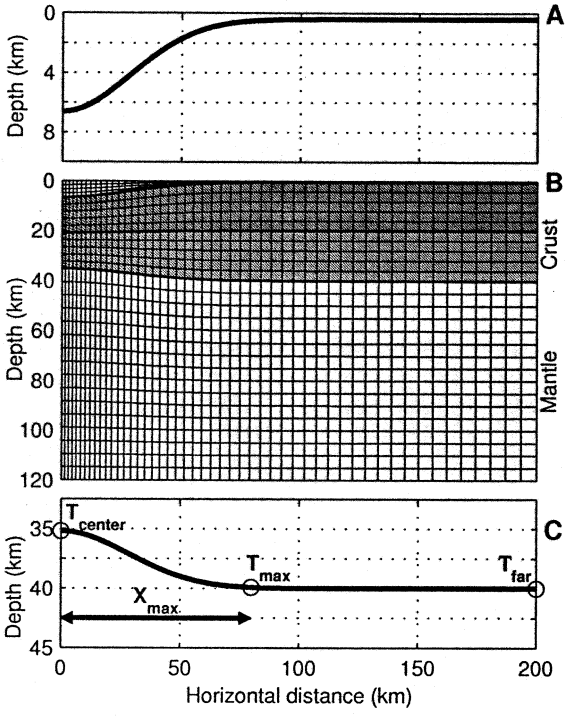

Fig. 1. Geometric configuration of a typical model. Since all models are symmetric only half of the basin structure is modeled. (A) The smooth shape of the top of basin basement. (B) The finite element mesh used in the solution of the heat transfer equation. (C) Shape of the crust–mantle transition. The locations of T_{center}, T_{far} and a typical location of $T_{\max}$ are also shown. $X_{\max}$ is the distance from basin center at which $T_{\max}$ is located.

where k_w is the thermal conductivity of pore water [11]. Consequently, thermal conductivities of the basin fill are functions of both lithology and basin depth.

The depth-integrated crustal heat production before stretching is denoted by Q_c. In the pre-rift situation the surface heat flow, Q_s, is the sum of background (mantle) heat flow, Q_b, and crustal heat production, $Q_s = Q_c + Q_b$. The crustal heat production is located in the heat-producing fraction, H_c, of the crust in which the heat production rate per unit volume is given by:

$$A_c = \frac{Q_c}{H_c Z_c} \quad (11)$$

After stretching and post-rift subsidence the inte-

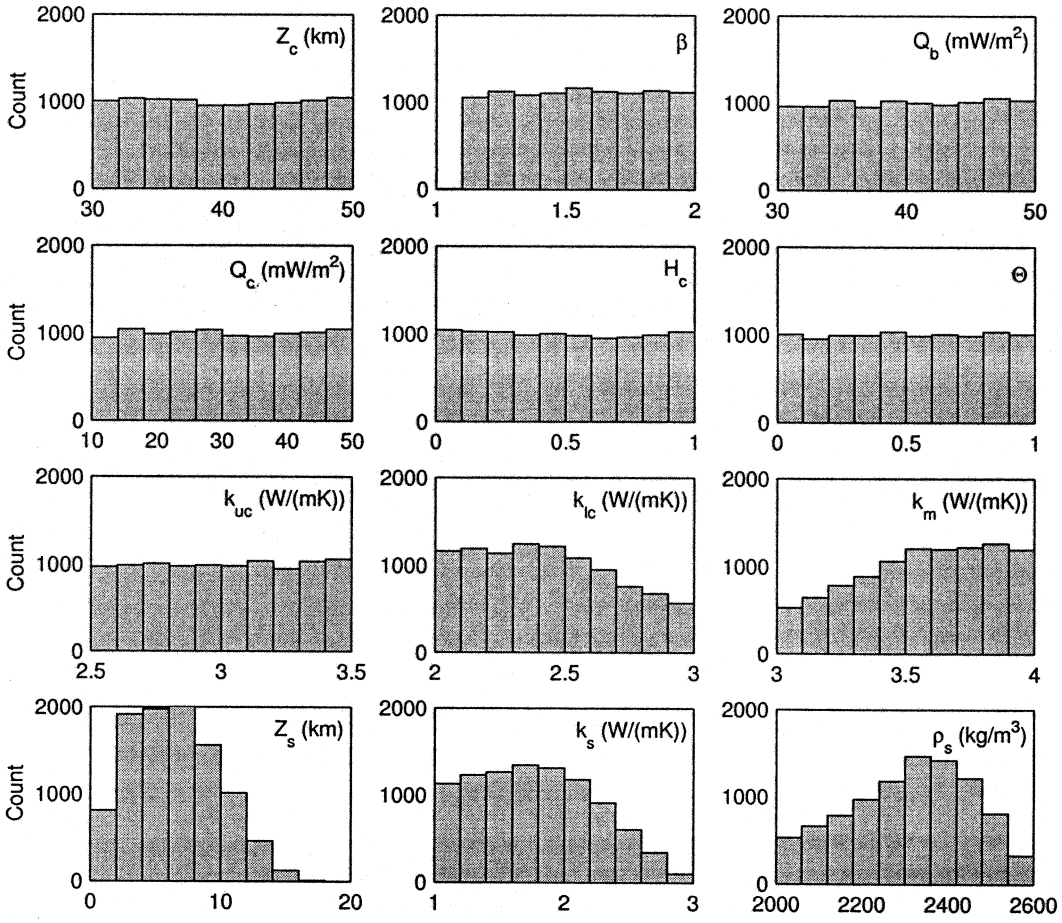

Fig. 2. Statistical distributions of model parameters. Z_c, β, Q_b, Q_c, H_c and Θ are uniformly distributed within the intervals given in Table 2. k_{uc}, k_{lc}, k_m, Z_s, k_s and ρ_s are constrained by relations given in the text.

grated heat production beneath the basin center is Q_c/β. The sedimentary heat production rate per unit volume is denoted by A_s. It is assumed that the mantle has no heat production.

The thermal conductivities of upper crust, lower crust and mantle are denoted by k_{uc}, k_{lc} and k_m, respectively. In the thermal modeling we have chosen to constrain these conductivities according to [12]:

$$k_{lc}<k_{uc}<k_m \tag{12}$$

Eqs. 2–12 define the geometry and parametric setting of a class of two-dimensional lithospheric models representing a wide variety of sedimentary basins all formed by uniform stretching followed by complete thermal relaxation and characterized by a smooth 'Gaussian' shape.

The Monte Carlo simulation is performed by repeatedly solving the steady-state heat transfer equation:

$$\frac{\partial}{\partial x}\left(k\frac{\partial T}{\partial x}\right)+\frac{\partial}{\partial z}\left(k\frac{\partial T}{\partial z}\right)=-A \tag{13}$$

where k is thermal conductivity and A is the heat production rate per unit volume. In the repeated calculations the fixed parameter values of Table 1 and random values of stochastic parameters within the intervals listed in Table 2 are adopted.

Table 2
Stochastic parameters and their range

Symbol	Parameter	Interval
Z_c	Crustal thickness	30–50 km
β	Stretching factor	1.1–2.0
Q_b	Background heat flow	30–50 mW/m^2
Q_c	Crustal heat flow contribution	10–50 mW/m^2
H_c	Heat-producing crust (frac.)	0.0–1.0
k_{uc}	Conductivity of upper crust	2.5–3.5 W/(mK)
k_{lc}	Conductivity of lower crust	2.0–3.0 W/(mK)
k_m	Conductivity of mantle	3.0–4.0 W/(mK)
Θ	Shale fraction	0.0–1.0

For explanations see Eqs. 2–12.

The heat transfer equation is solved using the finite element method [13] with the following boundary conditions: the left and right vertical axes are assumed to be axes of symmetry with no heat flow perpendicular to the axis. At the top of the model surface temperatures are assumed to be constant ($T_s = 0$°C) and at the bottom mantle heat flow (Q_b) is assumed laterally constant.

4. Results

Results from the Monte Carlo simulation are based on the calculated temperature distribution along the crust–mantle transition. The location of the maximum Moho temperature is of particular interest since the weakest mantle material is expected to be located just beneath this point. Fig. 1 defines the parameters of interest. The temperature beneath the basin center is denoted T_{center}. The temperature of the point farthest from the basin center is denoted T_{far} and represents the Moho temperature of the undisturbed lithosphere

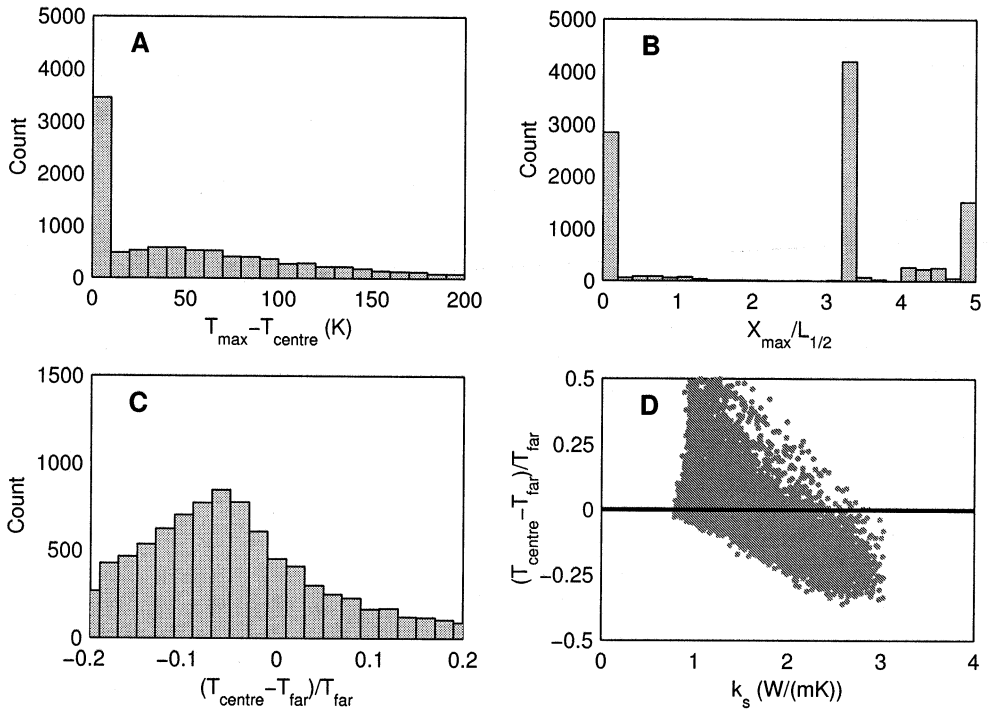

Fig. 3. Results of the one-dimensional modeling. (A) The distribution of absolute differences between T_{center} and T_{max}. T_{center} is seen often to equal T_{max}. (B) The distribution of X_{max} normalized to the characteristic basin half width. T_{max} is found either in the basin center or far from the basin. (C) The distribution of relative differences between T_{center} and T_{far}. Positive values indicate thermal weakening, negative values indicate thermal hardening. (D) The correlation between basin fill conductivities and relative differences between T_{center} and T_{far}. Above the horizontal line situations of thermal weakening are found.

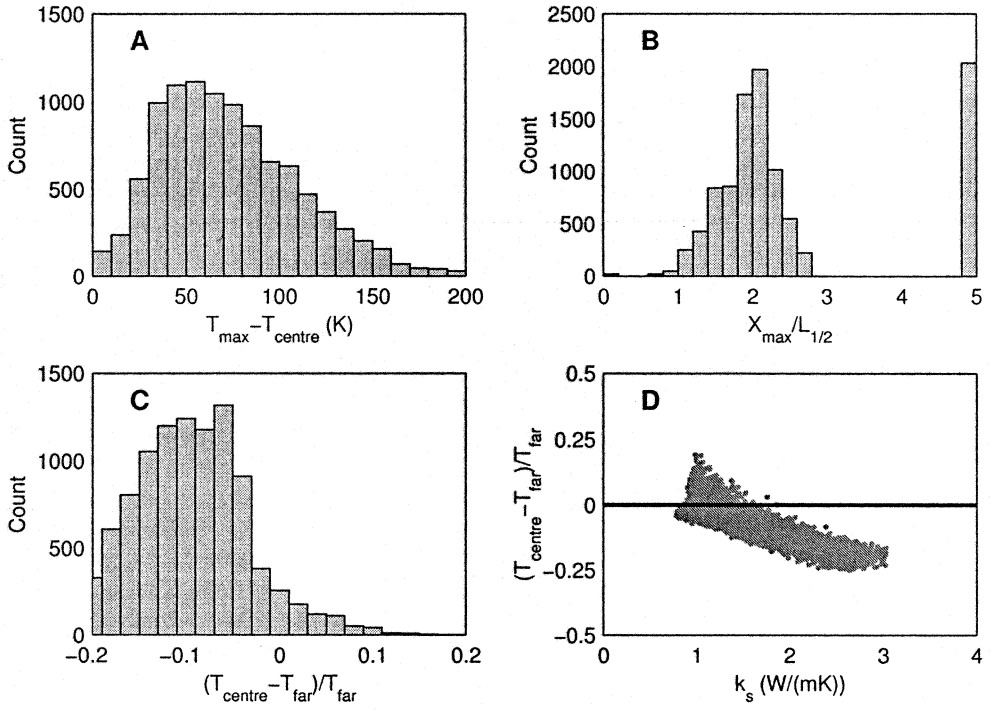

Fig. 4. Results of the two-dimensional modeling. (A) The distribution of relative differences between T_{center} and T_{max}. T_{max} is seen generally to exceed T_{center}. (B) The distribution of X_{max} normalized to the characteristic basin half width. X_{max} is generally seen to be twice the characteristic basin half width. (C) The distribution of relative differences between T_{center} and T_{far}. (D) The correlation between basin fill conductivities and relative differences between T_{center} and T_{far}. Situations of thermal weakening are found above the horizontal line only.

of the pre-rift situation. The maximum Moho temperature is denoted T_{max} and is found at distance X_{max} from the basin center.

The distribution of actually used model parameters is shown in Fig. 2. Values of crustal thickness (Z_c), stretching factor (β), background heat flow (Q_b), crustal heat production (Q_c), heat-producing crustal fraction (H_c), shale fraction (Θ) and upper crustal conductivity (k_{uc}) are uniformly distributed in the relevant intervals (see Table 2). The conductivities of lower crust and mantle are constrained by Eq. 12. The depth of basin center (Z_s), the conductivity of basin fill ($\langle k_s \rangle$), and the density of basin fill ($\langle \rho_s \rangle$) are calculated from Eqs. 3, 10 and 4, respectively. Basin depths range from 1 to 20 km with 6–8 km being the most frequent values. The total number of models is 10 000.

First of all, the results of Sandiford are reproduced by neglecting horizontal heat flow and thereby adopting the one-dimensional approximation. As is seen in Fig. 3A,B the temperature of the basin center represents the maximum Moho temperature in more than half of the 10 000 models. For later reference we also show the relative differences between T_{center} and T_{far} as histograms (Fig. 3C) and as a function of basin fill conductivities (Fig. 3D). These results emphasize that one-dimensional thermal modeling inevitably leads to the conclusion that thermal weakening dominates in sedimentary basins as suggested by Sandiford [5].

Fig. 4 shows the results of the two-dimensional thermal modeling. The Moho temperatures beneath the basin center (T_{center}) are now seen generally to differ from the maximum Moho temperature (T_{max}) by 0–20% (Fig. 4A). In a few cases T_{center} still equals T_{max} and in these cases $X_{max} = 0$. However, in by far the majority of cases, maximum Moho temperatures are now found beneath the basin flanks ($X_{max} \approx 2L_{1/2}$) (Fig. 4B). Com-

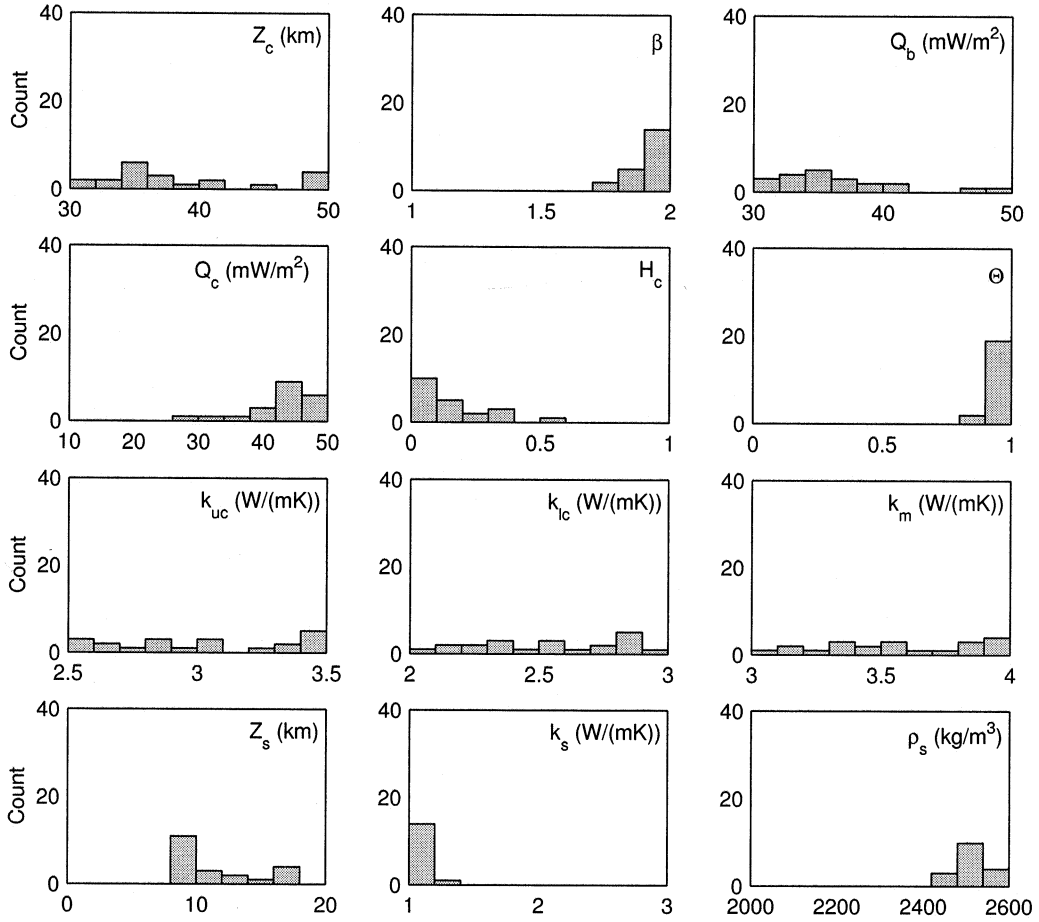

Fig. 5. The distribution of parameters related to class 1 models. T_{center} equals T_{max}. The class 1 models represent 0.2% of the model assemblage only and are characterized by large depths and extremely low conductivity sediments.

pared to the one-dimensional models the relative changes of Moho temperatures due to basin formation show a much clearer correlation with basin fill conductivities (Fig. 4D). This result indicates that the effect of thermal weakening becomes more dependent on low sedimentary conductivities when two-dimensional effects are considered.

The 10 000 models are divided into four classes as shown in Table 3 representing different thermal configurations. The parametric distribution related to each class is shown in Figs. 5–8.

For approximately 7% of the models temperatures of the uppermost mantle beneath the basin center increase as a consequence of basin formation, that is: $T_{far} < T_{center} \leq T_{max}$. These cases belong to class 1 or class 2.

Table 3
The 10 000 models are divided into four classes

Class	Thermal configuration	Fraction (%)
1	$T_{center} = T_{max}$	0.2
2	$T_{far} < T_{center} < T_{max}$	6.4
3	$T_{center} < T_{far} < T_{max}$	73.1
4	$T_{far} = T_{max}$	20.3

The four classes are defined by their thermal configuration. The fractional representation of each class is shown for $L_{1/2} = 40$ km.

Class 1 represents cases where thermal weakening causes the upper mantle beneath the basin center to be the weakest upper mantle material along the lithospheric profile. In these cases, sedimentary basins are able to invert by lithospheric pure shear-style compression. However, as shown in Fig. 5, these situations only appear in very deep basins ($Z_s \geq 8$ km) filled with shale-dominated sediments characterized by very low thermal conductivities ($k_s \leq 1.5$ W/mK). Even though the existence of such basins cannot be excluded, we do not consider them to be representative of the inverted basins in the alpine foreland.

In cases belonging to class 2 and class 3 the maximum Moho temperature is located at some point along the lithospheric profile between the basin center and the undisturbed lithosphere (at the right margin) representing the pre-rift situation. As already mentioned, the Monte Carlo simulation clearly indicates that the location of maximum Moho temperature is most likely to be related to the basin flank (Fig. 4B).

The class 2 models represent cases where, following basin formation, the Moho temperature increases beneath the basin center without becoming the maximum Moho temperature. Thus, in these situations the mantle beneath the basin center experiences thermal weakening. However, even

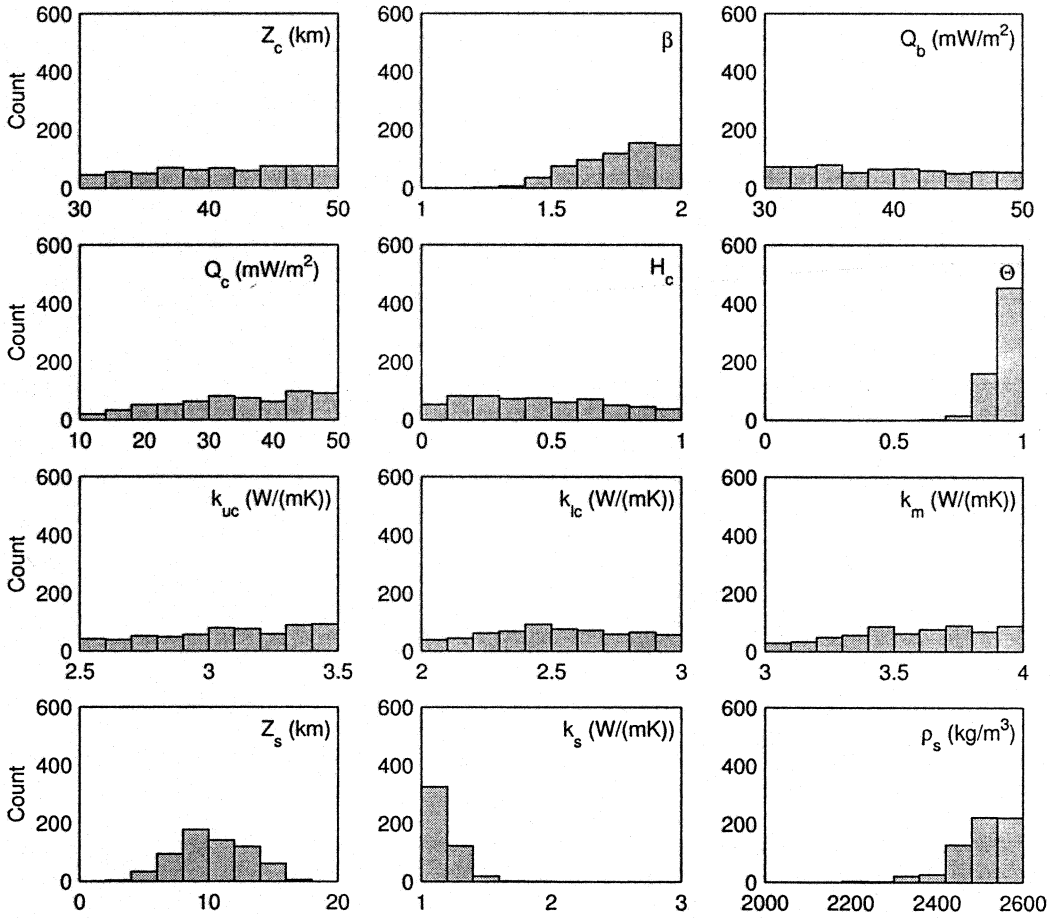

Fig. 6. The distribution of parameters related to class 2 models. T_{center} exceeds T_{far} but does not equal T_{max}. The class 2 models represent 6.4% of the model assemblage and like the class 1 models are characterized by large basin depths dominated by shaly sediments.

warmer mantle material exists outside the basin center and pure shear-style inversion is not an obvious consequence of the thermal weakening. 6.5% of the 10 000 models belong to class 2. As shown in Fig. 6 these models are characterized by very thick (approx. 10 km) shaly covers of sediments. Therefore, the class 2 models are still quite unusual basins.

Class 3 is by far the most representative class containing 73% of the models. In these frequently occurring situations the mantle beneath the basin center does not experience thermal weakening. Moho temperatures decrease due to decreasing burial depths and thermal hardening is the direct consequence of basin formation. The mantle beneath the flanks of the basin experiences thermal weakening and is the warmest and weakest mantle material in the region. Class 3 represents a wide range of models as seen in Fig. 7 with basin depths of 0–15 km filled with both shaly and non-shaly sediments.

Class 4, like class 1 and class 2, represents extreme situations. In these cases the maximum Moho temperature is found in the undisturbed lithosphere and here basin formation leads to a regional strength increase and thermal weakening is not a consequence of basin formation anywhere. As seen in Fig. 8 these situations emerge

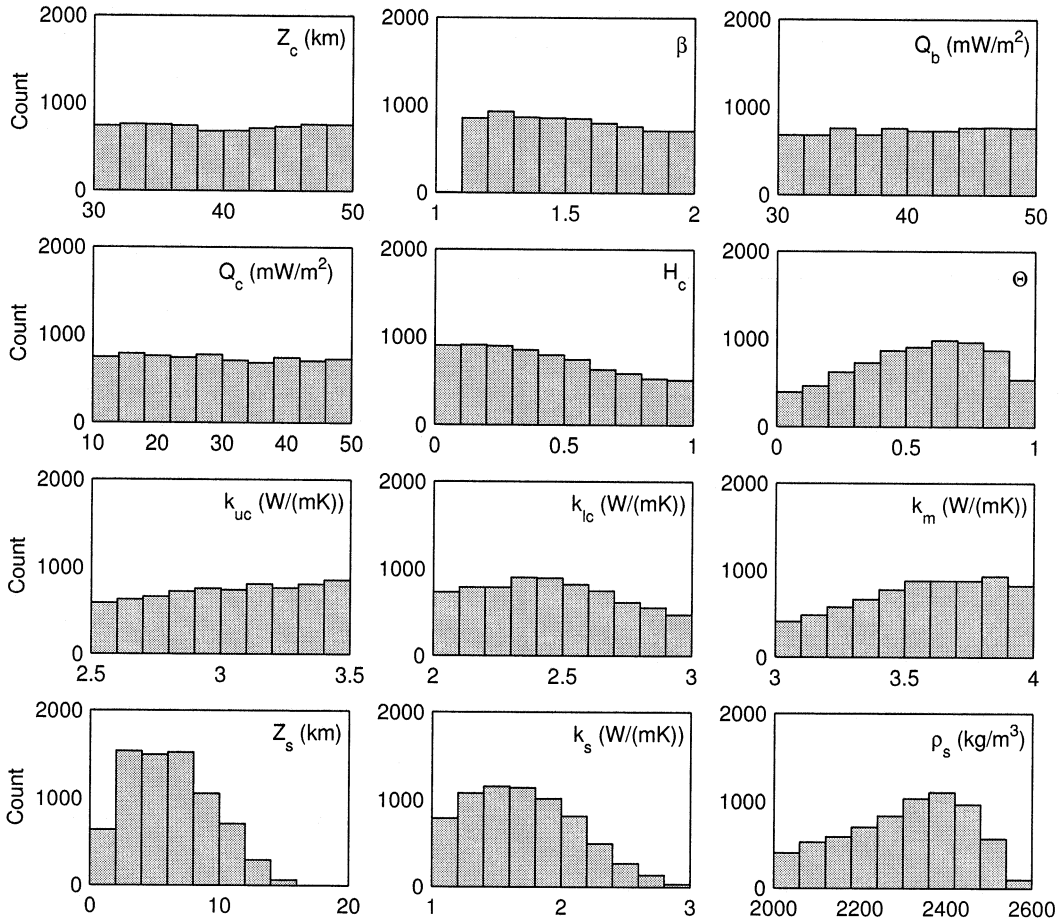

Fig. 7. The distribution of parameters related to class 3 models. T_{far} exceeds T_{center} but does not equal T_{max}. The class 3 models represent 73.1% of the model assemblage and are considered to comprise the most realistic models.

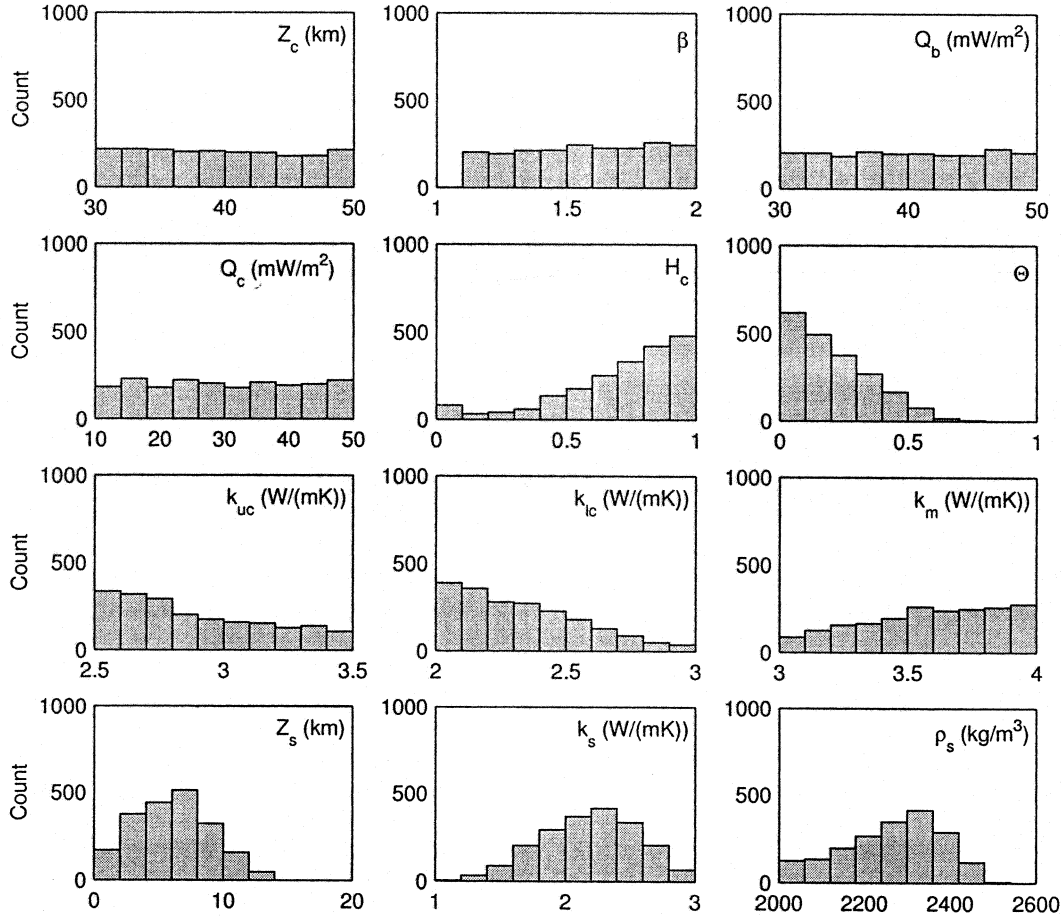

Fig. 8. The distribution of parameters related to class 4 models. T_{far} equals T_{max}. The class 4 models represent 20.3% of the model assemblage and are characterized by widely distributed crustal heat production and highly conductive sediments.

when the sediments are highly conductive ($k_s \approx k_{uc}$) and the heat production is widely distributed within the crust ($H_c > 0.5$).

The main result emerging from the two-dimensional stochastic modeling is that in all but extreme cases maximum Moho temperatures are found beneath basin flanks. Even if the basin center undergoes thermal weakening due to basin formation (in the sense that $T_{center} > T_{far}$ as in class 2) the upper mantle beneath the basin center is still relatively strong (since $T_{center} < T_{max}$) and thus thermal weakening of mantle material does not explain basin inversion. Instead these results support the conclusions of Ziegler et al. [3] and Negredo et al. [14] where the relative weakness of basin flanks also was suggested based on thermal studies of kinematic models.

5. Discussion

Fig. 9 elucidates how the effect of thermal refraction creates the large differences between the one- and two-dimensional cases of the former section. Shown in Fig. 9A are the surface heat flow profiles in the case of one- and two-dimensional thermal conduction for a model of class 3. The one-dimensional heat flow is rather constant, apparently because in this particular case the heat production rate of the sediment compensates for

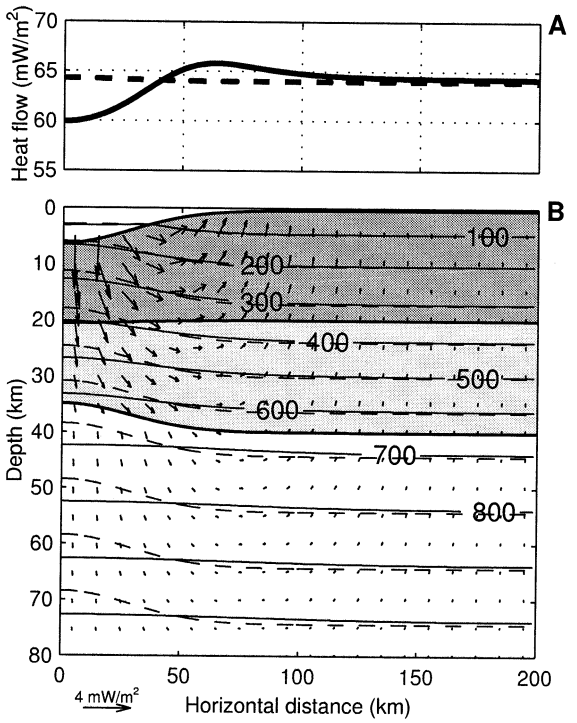

Fig. 9. Heat flow pattern in the one- and two-dimensional situations. (A) Surface heat flow densities. The broken line is obtained by one-dimensional conduction and the solid line is obtained by two-dimensional conduction. Two-dimensional conduction results in a heat flow low at the basin center and a heat flow high at the basin flanks. (B) Deviatoric heat flow pattern in the lithosphere obtained by taking the difference between heat flow vectors resulting from the two- and one-dimensional cases. Broken and solid lines represent isotherms resulting from the one-dimensional and two-dimensional approximations, respectively.

the heat production deficit of the thinned crust. The two-dimensional heat flow profile, however, exhibits a low in the basin and a high at the basin margin. These anomalies are caused by heat refraction mainly in the conductivity contrast of sediment and upper crust. Fig. 9B shows heat flux vectors obtained by taking the difference between the two-dimensional heat flux vector and its one-dimensional counterpart. This flow pattern clearly shows the retardation of heat flux below the thick sediments and the deviation of heat flux away from the central basin area and into the adjacent basement high. From examples like this we conclude that the frequent occurrence of Moho T_{max} in the vicinity of the basement flank is caused by a positive and relatively wide heat flux anomaly associated with the basin flank. This positive heat flux anomaly is caused by heat deviated away from the central basin area into the surroundings.

Actual detection of this refractive heat flow anomaly by observation of heat flow in boreholes would be problematic because of the common 10% uncertainty in heat flow determinations induced by uncertain thermal conductivity determinations and temperature measurements.

Clearly, the resulting deviations between one-dimensional models and two-dimensional models depend on the width of the relevant basin. In very wide basins thermal refraction beneath the basin center plays a less important role than beneath narrow basins, and the thermal state is well approximated by one-dimensional considerations. The role of the characteristic basin half width ($L_{1/2}$) has been examined in detail and the results are shown in Fig. 10. As expected, the number of class 1 situations is seen to increase as basin width

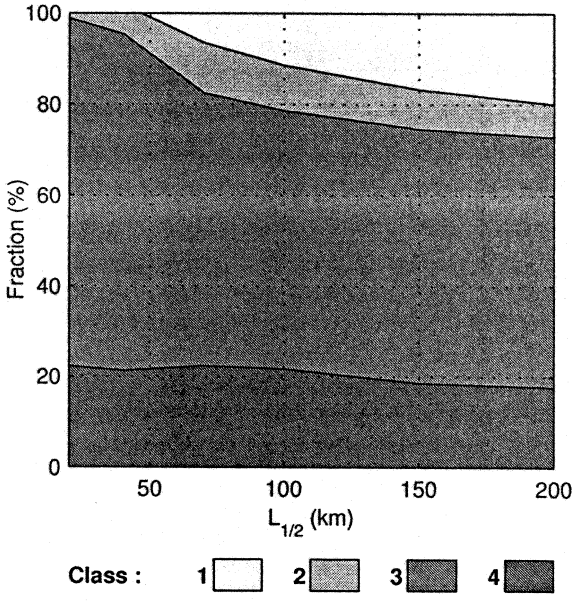

Fig. 10. Fractional representation of the four basin classes defined in Table 3 for varying basin widths. Only in very wide basins does the fractional representation of class 1 situations, characterized by complete thermal weakening, exceed 20%.

increases. But even for a basin characterized by a flank to flank distance of 400 km ($L_{1/2} \approx 100$ km) the maximum Moho temperature is only found beneath the basin center in 20% of the cases. In contrast to the number of class 1 models, the number of class 4 models is rather constant and thus independent of the basin width.

Consequently, in most cases, the weakest mantle material is, by thermal considerations only, most likely to be located beneath basin flanks even in wide basins. The direction of vertical displacement of crustal material in lithospheric stretching depends on the initial vertical positioning within the crust. In the upper part of the crust, which gets buried deeper during basin formation, nothing counteracts the process of thermal blanketing from the sediments. Below some level in the lower crust material becomes elevated in response to crustal thinning and here thermal blanketing is counteracted by a decreasing burial depth. This level is, however, generally found quite deep in the weak and ductile lower crust. Therefore the weakest crustal material is, by thermal considerations only, expected to be found beneath basin centers. This complex pattern is illustrated in Fig. 11 where contours of temperature changes following basin formation are shown for a typical model belonging to class 3. In this figure it is quite clear that the upper crust is heated while only a very narrow area of the mantle beneath the rift flanks experiences a small temperature increase. The mantle and deepest parts of the crust beneath the basin center experience a temperature decrease.

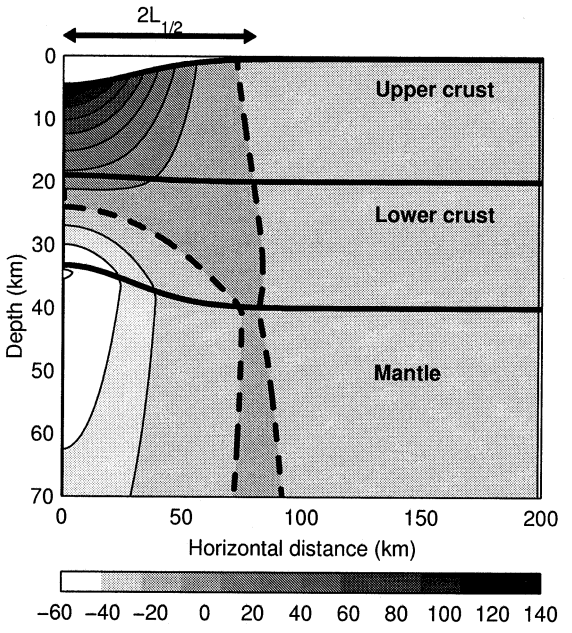

Fig. 11. Temperature changes induced by the basin-forming process for a typical model belonging to class 3. Negative temperature changes indicate cooling and positive heating. The temperatures of upper mantle material beneath the basin center decrease due to burial depth reduction. The upper crustal temperatures increase due to burial beneath low conductive sediments. The zero contour is represented by a dashed line. The area of slight temperature increase is seen to penetrate the mantle beneath the rift flanks. Beneath the basin the zone of temperature conservation is found in the lower crust.

Because Moho T_{max} is beneath the flanking highs the weakest parts of crust and mantle are laterally offset as illustrated in Fig. 12, where rheological profiles have been calculated using the two-dimensional temperature distribution of a typical situation of class 3 from the stochastic modeling. In the calculation of rheological profiles, steady-state creep stresses were found by Eq. 1 with creep parameters as given in Table 4. The yield strength, σ_y, was calculated from Murrel's extension of Griffith's criterion [6,10]:

$$\sigma_y = 12Tp^L \tag{14}$$

where p^L is the lithostatic pressure and T is a strength parameter which differs in extension and compression. The strength parameters are also given in Table 4.

This lateral offset between weakness therefore seems to facilitate a simple shear-type inversion with little or no mantle deformation beneath inverted basin centers. Exactly how the lithosphere responds to compression and how strains are distributed in the mantle is not clear from rheological profiles as in Fig. 12, however, since they assume depth-invariant strain rates. Instead, the natural response of a sedimentary basin in compression should be tested by the use of two- or three-dimensional dynamic models [2,6,10,11] which is not the subject of this paper.

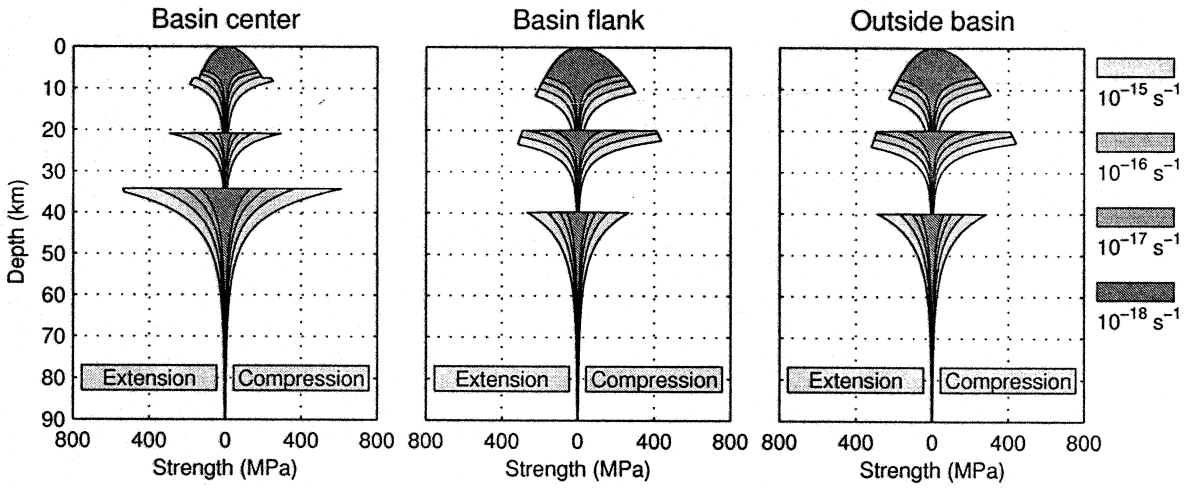

Fig. 12. Lithospheric rheological profiles calculated in the basin center, at the basin flank and far from the basin. The calculations were based on a typical two-dimensional temperature field and the assumption of depth-invariant strain rates. Each profile is shown for four different strain rates. The basin center is characterized by relatively strong mantle material and relatively weak crustal material. The weakest mantle material is found beneath the basin flanks.

6. Conclusions

Our study reveals that the equilibrium thermal structure of sedimentary basins generally is significantly influenced by deviation of heat from the central parts of the basins towards the basin flanks. This results in a heat flow low in the basin and a heat flow high at the margins. This heat flow high is responsible for the occurrence of the maximum Moho temperature beneath the basin flanks.

The occurrence of basin inversion demonstrates that sedimentary basins can be weak even a long time after their formation. This paper has investigated whether the equilibrium thermal structure of a sedimentary basin in itself can produce a rheological structure, which facilitates compressional inversion. By Monte Carlo simulation of the thermal structure of groups of 10 000 extensional sedimentary basins we find that for the vast majority of sedimentary basins the weakest upper mantle occurs in the vicinity of the basin flanks. The crust is weakest in the basin center due to thermal elevation of the brittle–ductile transition zones in the crust and the presence of weak sediments. Only in very few models is the Moho temperature found to be at its maximum beneath the center of the basin. These models appear to require an extraordinary fortuitous combination of (1) very thick sedimentary cover ($Z_s > 8$ km), (2) extremely low conductive sediments ($k_s < 1.5$ W/mK) and (3) very shallow and localized crustal

Table 4
Rheological parameters used to calculate steady-state creep stress and yield strength for rocks in extension and compression

Symbol	Parameter	Mantle	Lower crust	Upper crust	Sediments
n	Creep parameter	4.48	3.20	3.10	3.10
B	Creep parameter	0.2628 MPa s$^{1/n}$	12.28 MPa s$^{1/n}$	208.0 MPa s$^{1/n}$	208 MPa s$^{1/n}$
Q	Creep parameter	498 kJ/mol	239 kJ/mol	135 kJ/mol	135 kJ/mol
T^e	Tensile strength	26.2 MPa	13.1 MPa	13.1 MPa	13.1 MPa
T^c	Compressive strength	52.4 MPa	26.2 MPa	26.2 MPa	17.5 MPa

Creep parameters are from Copra and Paterson [15] for mantle (wet dunite), from Shelton and Tullis [16] for lower crust (anorthosite), and from Paterson and Luan [17] for upper crust and sediments (wet quartzite).

radiogenic heat production. In those extreme cases localized basin inversion in pure shear and the formation of marginal basins may result from compression. In all other cases a lateral offset between crustal and mantle weakness exists. Whether such a structure inverts in compression is not trivial and must be tested by the use of dynamic rheological models. The fact that basin inversion is characterized by uplift of basin centers and the formation of marginal basins points in the direction of highly localized upper and lower crustal deformation [2]. From this study and two-dimensional dynamic modelling [2,6] we suggest that pre-existing structural weakness plays a more important role in the process of basin inversion than thermal weakening. Thus, the conclusion is that thermal weakening alone does not explain basin inversion in any satisfactory way.

Acknowledgements

The authors thank Mike Sandiford for helpful correspondence and useful comments. Giorgio Ranalli and Ritske Huismans are acknowledged for very constructive reviews improving the manuscript considerably.*[FA]*

References

[1] G.D. Williams, C.M. Powell, M.A. Cooper, Geometry and kinematics of inversion tectonics, Geol. Soc. Spec. Publ. 44 (1989) 3–15.
[2] S.B. Nielsen, D.L. Hansen, Physical explanation of the formation and evolution of inversion zones and marginal basins, Geology 28 (2000) 875–878.
[3] P.A. Ziegler, S. Cloetingh, J.D. vanWees, Dynamics of intra-plate compressional deformation the alpine foreland and other examples, Tectonophysics 252 (1995) 7–59.
[4] P.A. Ziegler, Geological Atlas of Western and Central Europe, Shell International Petroleum Maatschappij B.V., The Hague, 1987.
[5] M. Sandiford, Mechanics of basin inversion, Tecotonophysics 305 (1999) 109–120.
[6] D.L. Hansen, S.B. Nielsen, H. Lykke-Andersen, The post-Triassic evolution of the Sorgenfrei-Tornquist zone – results from thermo-mechanical modeling, Tectonophysics 328 (2000) 245–267.
[7] L. Gemmer, S.B. Nielsen, 3-D inverse modelling of the thermal structure and implications for lithospheric strength in Denmark and adjacent areas of north west Europe, Geophys. J. Int. 147 (2001) 141–154.
[8] M. Fernandez, G. Ranalli, The role of rheology in extensional basin formation modelling, Tectonophysics 282 (1997) 129–145.
[9] G. Ranalli, Rheology of the Earth, Chapman and Hall, London, 1995.
[10] J. Braun, C. Beaumont, Styles of continental rifting: Results from dynamic models of lithospheric extension, in: C. Beaumont, A.J. Tankard (Eds.), Sedimentary Basins and Basin-Forming Mechanisms, Can. Soc. Pet. Geol. Mem., 1987.
[11] P.A. Allen, J.R. Allen, Basin Analysis – Principles and Applications, Blackwell Scientific Publications, London, 1990.
[12] Niels Balling, Heat flow and thermal structure of the lithosphere across the baltic shield and northern tornquist zone, Tectonophysics 244 (1995) 13–50.
[13] J.E Akin, Application and Implementation of Finite Element Methods, Academic Press, London, 1989.
[14] A.M. Negredo, M. Fernandez, H. Zeyen, Thermo-mechanical constraints on kinematic models of lithopheric extension, Earth Planet. Sci. Lett. 134 (1995) 87–98.
[15] P.N. Chopra, M.S. Paterson, The experimental deformation of dunite, Tectonophysics 78 (1981) 453–473.
[16] G. Shelton, J. Tullis, Experimental flow laws for crustal rocks, EOS Trans. Am. Geophys. Union 62 (1981) 396.
[17] M.S. Paterson, F.C. Luan, Quarzite rheology under geological conditions, in: R.J. Knipe, E.H. Rutter (Eds.), Deformation Mechanisms, Rheology and Tectonics, Geol. Soc. Spec. Publ. 54 (1990) 299–307.